11th International Conference on Fracture Mechanics of Concrete and Concrete Structures
FraMCoS-11
J. M. Chandra Kishen, A. Ramaswamy, S. Ray and R. Vidyasagar (Eds)
https://doi.org/10.21012/FC11.092367

NUMERICAL MODELING OF GFRP BAR-REINFORCED CONCRETE SLABS-ON-GROUND SUBJECTED TO CONCENTRATED LOADS AT THE EDGE AND CORNER

MOHAMMED FASIL[*], MUHAMMAD K. RAHMAN[†], MESFER M. AL-ZAHRANI[‡] AND MOHAMMED A. AL-OSTA[§]

[*] Civil and Environmental Engineering Department
King Fahd University of Petroleum and Minerals, Dhahran 31261, Saudi Arabia
e-mail: mohammed.fasil@kfupm.edu.sa

[†]Interdisciplinary Research Center for Construction and Building Materials
King Fahd University of Petroleum and Minerals, Dhahran 31261, Saudi Arabia
e-mail: mkrahman@kfupm.edu.sa

[‡]Civil and Environmental Engineering Department
King Fahd University of Petroleum and Minerals, Dhahran 31261, Saudi Arabia
e-mail: mesferma@kfupm.edu.sa

[§]Interdisciplinary Research Center for Construction and Building Materials
King Fahd University of Petroleum and Minerals, Dhahran 31261, Saudi Arabia
e-mail: malosta@kfupm.edu.sa

Key words: Glass fiber-reinforced polymer (GFRP), punching shear, numerical simulation

Abstract: Major advances in the utilization and standardization of glass fiber-reinforced polymer (GFRP) bars as reinforcing material in structural members were witnessed in the past two decades. Due to the properties of GFRP bars, such as the linear stress-strain response, a brittle mode of tensile failure, and concrete-GFRP bond behavior, there is a substantial need for experimental data and numerical analyses to characterize the behavior of GFRP bars embedded in concrete structural members. Addressing this requirement, this study focuses on the punching shear capacity of GFRP bar-reinforced concrete slabs-on-ground which is primarily designed for shrinkage and crack width control, through experimental studies and numerical investigations in ABAQUS. This study fills the gap in the state-of-the-art by reporting the outcomes of numerical parametric studies conducted to examine the performance of GFRP bar-reinforced concrete slabs-on-ground subjected to center, edge, and corner loads. The numerical model developed in this study was calibrated based on the load-displacement responses of the specimens from the experimental program. Upon validation, parametric studies were conducted to investigate the influence of variables such as concrete strength, reinforcement ratio, and rebar grid location, and a comparison with existing design equations in standards and literature was made.

1 INTRODUCTION

Slabs-on-ground are used extensively in structures such as industrial floors, walkways, storage areas, and stormwater channels. These slabs are generally subjected to both environmental and structural loads from

moving vehicles such as maintenance trucks, and loaded forklifts. The environmental loads when the concrete slabs are exposed to ambient condition generates the physical mechanism arising from moisture diffusion from fresh concrete and causing drying shrinkage tensile stresses and associated cracking when the tensile stresses exceed the tensile strength of concrete. In steel-reinforced concrete slabs-on-ground, these cracks are potential pathways for the ingress of chemicals and chlorides which attack the steel reinforcement and cause corrosion. The non-metallic glass fiber-reinforced polymer (GFRP) bars emerged as a potential replacement for corrosion-prone steel bars in harsh and aggressive environments [1,2]. It is now being utilized in several applications such as bridge decks, marine structures, sea walls, and channels [2–4]. Being a corrosion-free and lightweight material, with high tensile strength, it can provide a service life of over 100 years, although it has prominent drawbacks including low elastic modulus and possible rupture in creep.

The slabs-on-ground are generally reinforced with steel reinforcement grids at the exposed top surface to cater to the shrinkage and thermal stresses [5]. Being supported on grade over the entire area, the latter acting as springs attached to the slab, it is expected that the loads due to occasional maintenance and goods trucks can be resisted safely. In industrial floors and warehouses, these slabs may be subjected to higher loads more frequently and it is necessary to ensure that the slab thickness and reinforcement are enough to cater for the concentrated loads. For preventing shrinkage-induced cracks and for concreting, it is essential to incorporate joints in the grade-supported slabs at selected intervals [6]. The edges and corners of the slabs-on-ground are critical locations, where the behavior under a concentrated wheel load is entirely different from the application of these wheel loads at the points away from the edges and the corners. The corners in particular are prone to lifting and moving into the grade which causes cracking at the corners. The load at the center and edges of the slab causes tensile cracks at the bottom and the sides of the slabs and the failure takes place by the punching of load through the slab [7].

When the concentrated load is placed at the corner, the corner segment of the slab behaves as a cantilever resulting in the formation of the crack.

2 EXPERIMENTAL PROGRAM

To ascertain the punching shear capacity of a slab-on-ground reinforced with GFRP bars, an experimental program was conducted by the authors to investigate the punching shear capacity of slabs-on-ground reinforced with GFRP and steel rebar grids [7]. Two types of GFRP bars: sand-coated (SC) and ribbed (RB), and conventional ribbed steel (ST) bars were used as reinforcement to construct seven reinforced concrete slabs-on-ground (Figure 1). The properties of the reinforcing bars used in the experimental program are listed in Table 1. The concrete used in used was found to have a 28-day compressive strength of 34.5 MPa and split tensile strength of 2.6 MPa.

(a) SC: sand-coated GFRP

(b) RB: ribbed GFRP

(c) ST: ribbed steel

Figure 1: Reinforcing bars

Table 1: Mechanical properties of reinforcing bars

Property	SC	RB	ST
Guaranteed tensile strength (MPa)*	900.2	870.9	520 (yield)
Young's Modulus (GPa)	43.9	48.4	209
Diameter (mm)	13.5	13.7	12.7

The results from seven slabs tested in the experimental program conducted by the authors have been reported in the present study. Slabs of dimensions 1.5 × 1.5 m^2 in plan

and with a thickness of 150 m were used. The test matrix of the experimental program is shown in Table 2. Spacings of 200 mm and 300 mm were used in the study (Figure 2). Two rebar grid positions were used in the study: "top-third" with a clear cover of 50 mm from the top surface of the slab, and "mid-depth" with the rebar grid placed at the mid-depth of the slab-on-ground specimen. The experimental setup with concentrated loads applied at the corner of the slab is shown in Figure 3 (a). The three locations of concentrated load applications are shown in Figure 3 (b).

Table 2: Experimental program: test matrix

Sl.	Slab Name	Rebar type	Rebar spacing (mm)	Rebar grid location	Loading location
1	SC-200	SC	200	Top	Center
2	SC-300	SC	300	Top	Center
3	RB-200-M	RB	200	Mid	Center
4	RB-200-EDGE	RB	200	Top	Edge
5	RB-300-CORNER	RB	300	Top	Corner
6	ST-200	ST	200	Top	Center
7	ST-300	ST	300	Top	Center

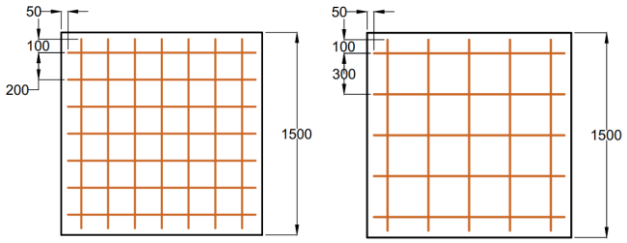

(a) 200 mm c/c (b) 300 mm c/c

Figure 2: Schematic: experimental specimens

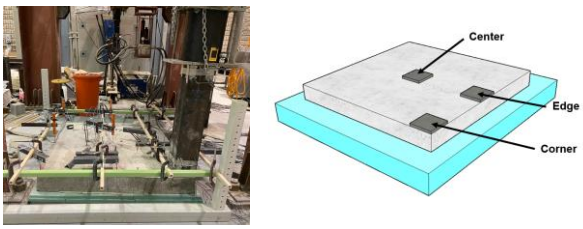

(a) test setup: corner loading (b) loading locations

Figure 3: Experimental testing

The modes of failure of the GFRP bar-reinforced concrete slabs-on-ground tested are shown in Figure 4. Failure in slabs loaded at the center was characterized by a punching cone and several cracks developing from the point of loading. The edge-loaded slab, RB-200-EDGE exhibited a half punching cone and three cracks developing from the point of loading. In the corner loaded slab, RB-300-CORNER, on the contrary, a flexural mode of failure was observed. The failure was brittle and no cracks were developed from the point of loading. The load-deformation responses for the loads applied at the center, corner, and edge locations are shown in Figure 5. The cracking and ultimate failure loads and their corresponding displacement are shown in Table 3.

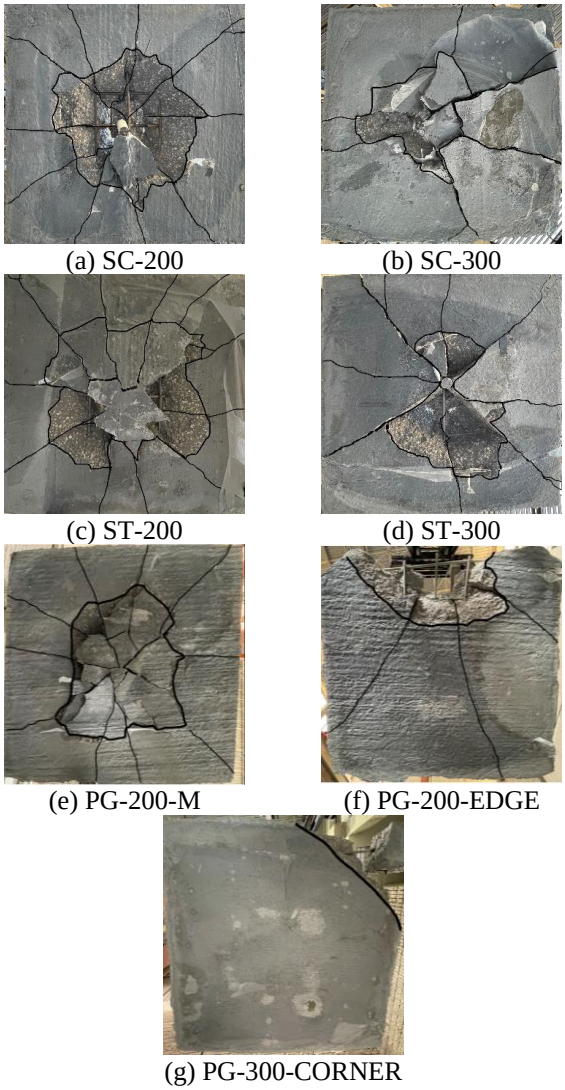

(a) SC-200 (b) SC-300

(c) ST-200 (d) ST-300

(e) PG-200-M (f) PG-200-EDGE

(g) PG-300-CORNER

Figure 4: Failure modes of experimental specimens

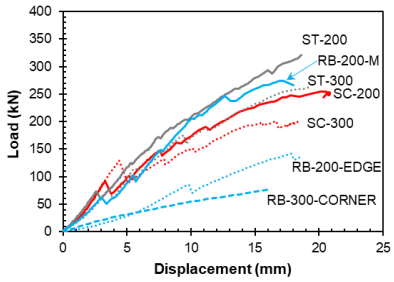

Figure 5: Load-deflection response of slabs-on-ground tested in the experimental program

Table 3: Experimental results: cracking and ultimate loads

Slab	Cracking		Ultimate	
	Load (kN)	Deflection (mm)	Load (kN)	Deflection (mm)
SC-200	92	3.2	255	20.7
SC-300	129	4.2	254	24.8
RB-200-M	62	3.0	271	16.2
RB-200-EDGE	85	9.6	226	-
RB-300-CORNER	-	-	132	6.4
ST-200	74	2.5	319	18.5
ST-300	79	3.7	268	19.6

3 FINITE ELEMENT SIMULATION OF SLAB

FE modeling is a powerful tool for simulating the experimental tests and to capture numerically the load-deflection response of the slabs tested. Reinforced concrete slabs resting on an XPS subbase simulating the soil were developed in ABAQUS CAE 2020, using the dynamic explicit module. The loading plate and the XPS subbase were modeled as solid homogenous parts and meshed using element type C3D8R (8-noded reduced integration hexahedral). The concrete slab was modeled using the element T3D4 (4-noded tetrahedral). The rebars were modeled as T3D (one-dimensional truss) elements.

The concrete damage plasticity (CDP) model in ABAQUS was used to model inelastic and damage behavior in concrete. The concrete compression stress-strain relation was developed using the fib Model code [8], while the tensile stress-strain response was modeled using the Wahalathantri et al. [9] model. Concrete damage in compression and tension was modeled using the Birtel and Mark model [10]. The extruded polystyrene (XPS) subbase was modeled as a crushable foam. The stress-strain responses of concrete, rebars, and the XPS foam are shown in Figure 7. The behavior of the XPS foam is compared with other types of subgrades including soft clay/loose sand, dense sand with gravel, and dense sand [11,12]. The behavior of the XPS foam closely matches that of dense compacted sand, thus simulating the actual soil subgrade.

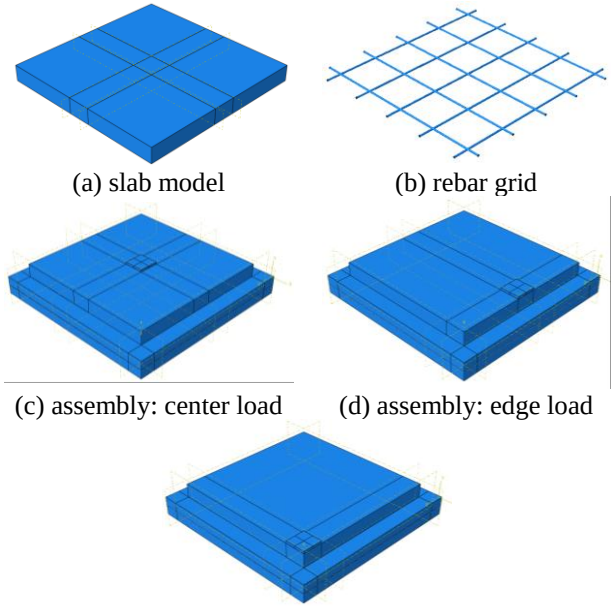

(a) slab model (b) rebar grid

(c) assembly: center load (d) assembly: edge load

(e) assembly: corner load

Figure 6: Geometry of numerical models in ABAQUS

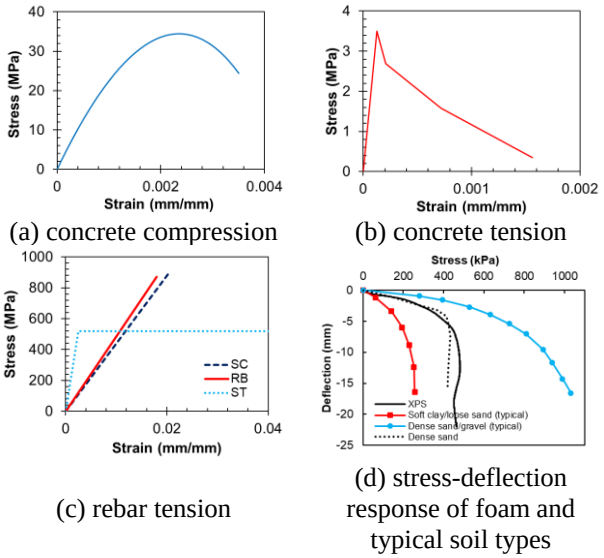

(a) concrete compression (b) concrete tension

(c) rebar tension (d) stress-deflection response of foam and typical soil types

Figure 7: Stress-strain relations

3.1 Calibration and validation

The parameters of the finite element model were calibrated to match the load-displacement response of the SC-200 slab specimen reinforced with the sand-coated (SC) bars spaced at 200 mm on the center, as shown in Figure 8 (a). The robustness of the numerical model, the predicted load-displacement responses of the slabs SC-300, RB-200-M, RB-200-EDGE, RB-300-CORNER, ST-200, and ST-300 were compared with the experimental results using the calibrated parameters developed for SC-200 (Figure 8 (b to g)).

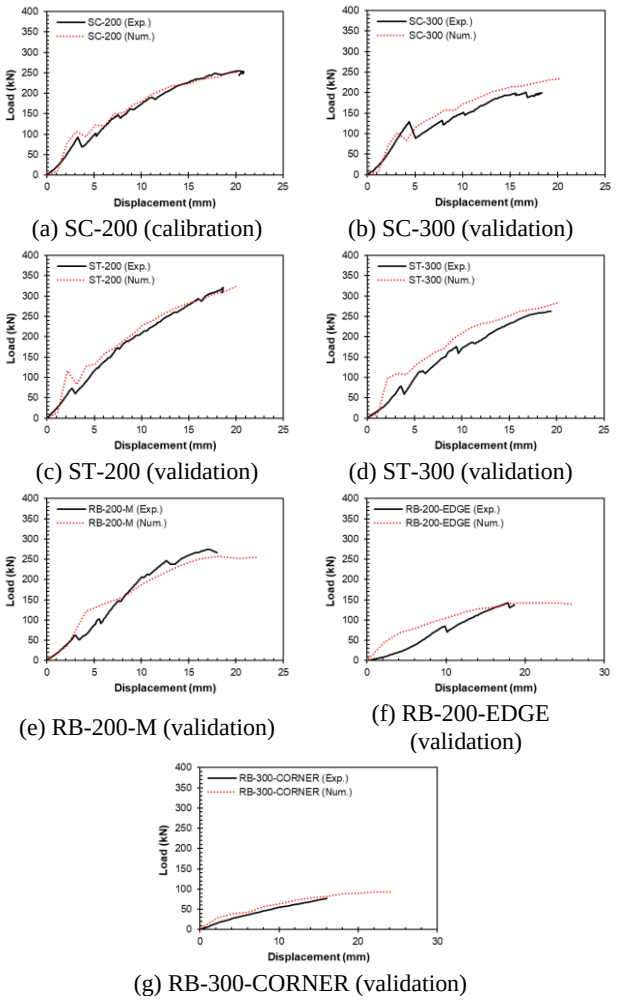

(a) SC-200 (calibration)
(b) SC-300 (validation)
(c) ST-200 (validation)
(d) ST-300 (validation)
(e) RB-200-M (validation)
(f) RB-200-EDGE (validation)
(g) RB-300-CORNER (validation)

Figure 8: Calibration and validation of the numerical model

The finite element simulations and the load-displacement response show that a reasonably good agreement was obtained between the numerical and experimental results, making the developed model suitable for numerical parametric studies. The effects of parameters such as concrete strength (compression and tension), rebar spacing, slab thickness, and secondary rebar grids were investigated

4 NUMERICAL PARAMETRIC STUDIES

Large-scale experimental tests can be carried out only on a limited number of specimens. FE simulation provides a powerful tool for assessing the response of the slabs under concentrated load with various parameters.

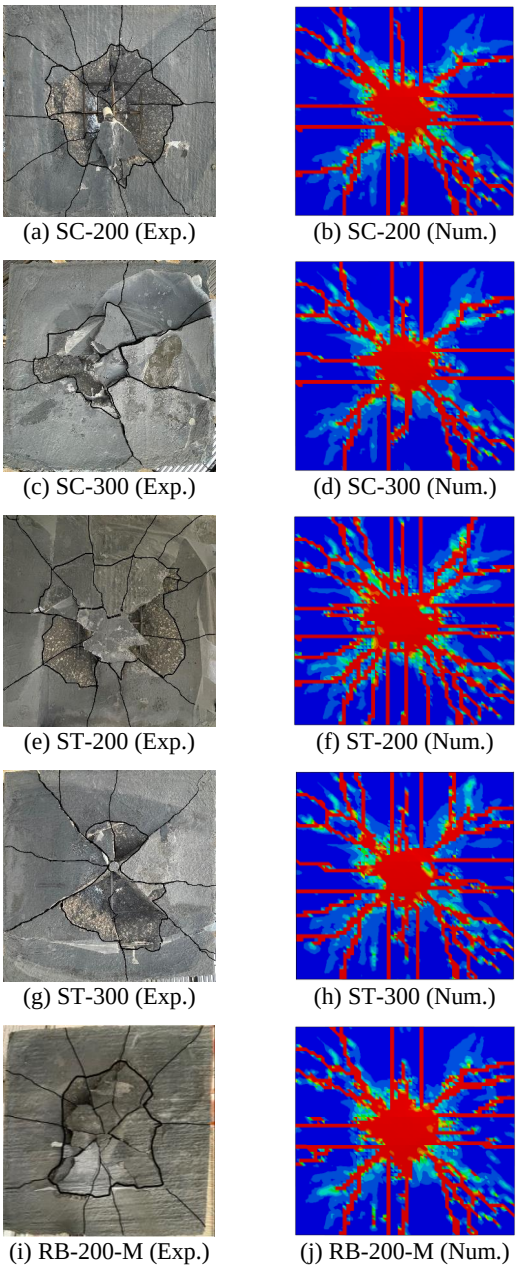

(a) SC-200 (Exp.)
(b) SC-200 (Num.)
(c) SC-300 (Exp.)
(d) SC-300 (Num.)
(e) ST-200 (Exp.)
(f) ST-200 (Num.)
(g) ST-300 (Exp.)
(h) ST-300 (Num.)
(i) RB-200-M (Exp.)
(j) RB-200-M (Num.)

(k) RB-200-EDGE (Exp.)

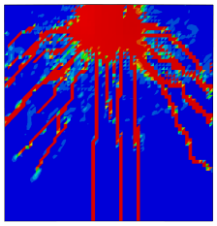

(l) RB-200-EDGE (Num.)

(m) RB-300-CORNER (Exp.)

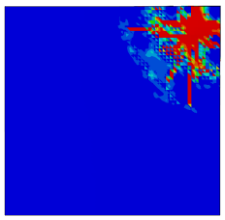

(n) RB-300-CORNER (Num.)

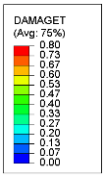

(o) Legend: concrete tension damage, d_t

Figure 9: Comparison of experimental and numerical failure modes

The FE model validated for capturing the selected actual experimental response was used to conduct parametric studies to assess the following aspects:

4.1 Effect of concrete compressive strength

The effect of concrete compressive strength on GFRP bar-reinforced concrete slabs-on-ground subjected to edge and corner loads was investigated by varying the concrete compressive strengths of 15 MPa, 25 MPa, 34.5 MPa (experimental value), 45 MPa, and 55 MPa in a slab with sand-coated (SC) bars with 200 mm spacing, loaded at edge and corner points using the validated finite element model. In the parametric studies on edge-loaded models, it is observed from Figure 10 (a) that the upto a load of 110 kN, no significant differences in the response were observed. However, beyond this point, the effect of concrete strength was very apparent. Upon increasing the concrete compressive strength from 15 MPa to 55 MPa, the ultimate load-carrying capacity of the slab at the edges was found to rise from 127 kN to 152 kN. However, in the case of corner-loaded slabs (Figure 10 (b)), the slab with 15 MPa concrete, strength and response was notably different than the slabs with concrete strength varying from 25 MPa to 55 MPa. The effect of variation of various concrete compressive strengths on slabs-on-ground loaded at edges and corners are plotted in Figure 10 (c).

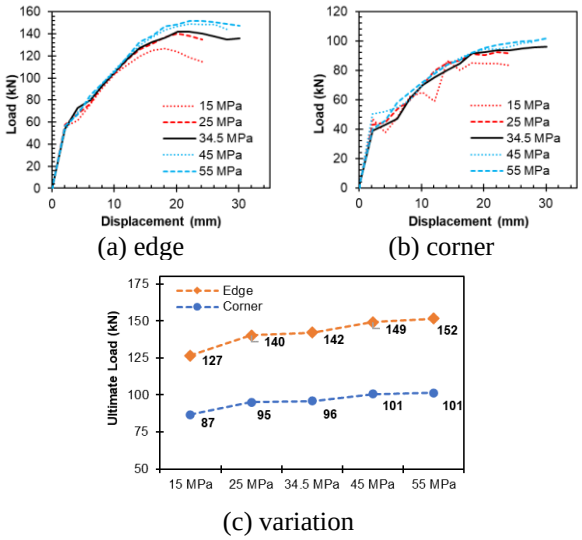

(a) edge (b) corner

(c) variation

Figure 10: Parametric investigations: effect of concrete compressive strength

4.2 Effect of concrete tensile strength

The concrete tensile strength was found to play a critical role in the stiffness and load-carrying capacity of GFRP bar-reinforced concrete slabs-on-ground subjected to edge and corner loads. The effect of concrete tensile strength was studied varying the tensile capacity of concrete from 1.5 MPa to 3.5 MPa. In the edge-loaded concrete slab models, the load-deflection response was found to be similar from the origin until a load of approximately 56 kN (Figure 11 (a)). Beyond this point, the influence of the tensile strength of concrete was evident. Upon increasing the tensile capacity of concrete from 1.5 MPa to 3.5 MPa, the punching load capacity was found to increase by 20.5%, as shown in Figure 11 (c). The superiority of the higher tensile strength of concrete was also observed in the corner-loaded slabs (Figure 11 (b)). Increasing the tensile strength of concrete from 1.5 MPa to 3.5 MPa, the punching load

capacity was found to increase by 17%, as shown in Figure 11 (c).

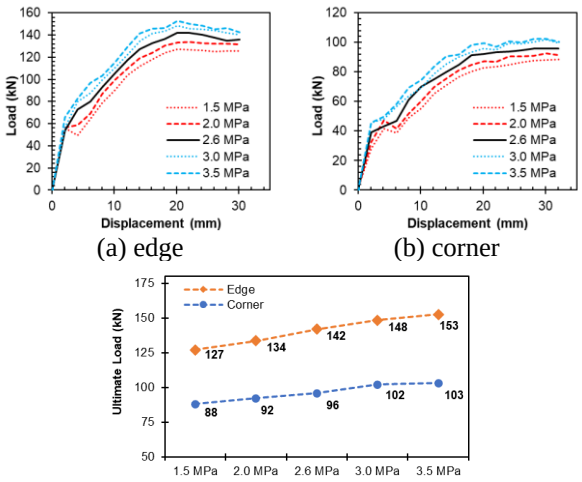

(a) edge (b) corner

(c) variation

Figure 11: Parametric investigations: effect of concrete tensile strength

4.3 Effect of rebar spacing

The rebar spacing in reinforced concrete slabs controls the number of bars that are activated during the composite action of the members. The influence reinforcement ratio was studied using the validated numerical model to simulate spacing of 100 mm, 150 mm, 200 mm (control), 250 mm, and 300 mm, corresponding to the reinforcement ratios of 0.95%, 0.63%, 0.48%, 0.38%, and 0.32%, respectively. Upon decreasing the spacings in the slab from 300 mm to 250 mm, 200 mm, 150 mm, and 100 mm, the load-carrying capacity of the slabs at the edge was found to increase by 0%, 4.4%, 11%, and 24%, following a non-linear rate of strength increment (Figure 12 (a and c)).

An interesting phenomenon was observed in the corner-loaded slab models (Figure 12 (b)). All models, except the slab with 250 mm spacing were found to follow the same trend of load-deflection response as in edge-loaded models. The slab with 250 mm was found to perform inferior to 300 spacing when loaded at the corner.

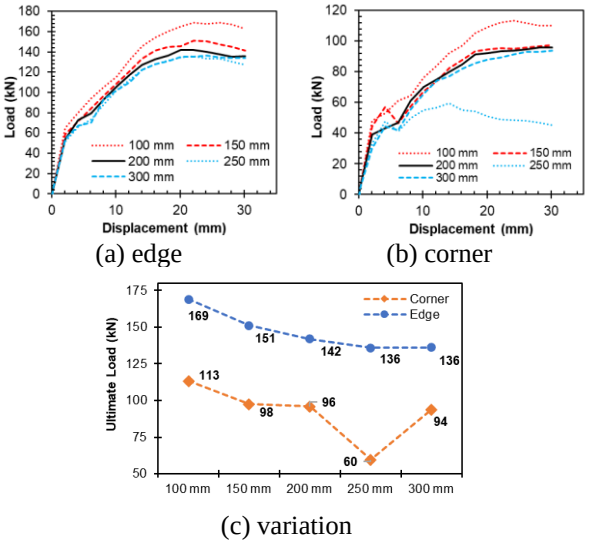

(a) edge (b) corner

(c) variation

Figure 12: Parametric investigations: effect of rebar spacing

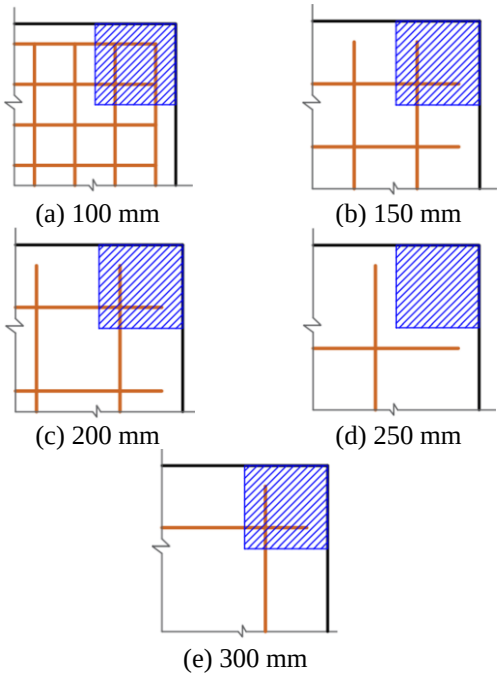

(a) 100 mm (b) 150 mm

(c) 200 mm (d) 250 mm

(e) 300 mm

Figure 13: Location of the loading plate and the rebar grids at various spacings

The reason for this interesting observation points to the importance of strengthening of corners of slabs-on-ground which are expected to sustain concentrated loads. When the GFRP bar grids were developed in ABAQUS, care was taken to make sure that the rebars were placed symmetrically in the slabs, while maintaining a cover of 50 mm from the edge faces. During this exercise, all reinforcing grids, except the one with 250 mm had rebars

right below the location of the loading plate located at the corner, as shown in Figure 13. This highlights the importance of strengthening the corners in reinforced concrete slabs-on-ground.

4.4 Effect of slab thickness

According to the purpose of the slab-on-ground structure to be constructed, the thickness can vary significantly. Higher thicknesses are generally adopted for slabs expected to be subjected to high-impact vehicular loads. To investigate the effect of slab thickness on the punching load capacity of GFRP bar-reinforced concrete slabs-on-ground, FE models with slab thicknesses of 100 mm, 150 mm, 200 mm, and 250 mm were simulated. A clear cover of 50 mm to the rebar grid from the top surfaces of the models was maintained in all cases.

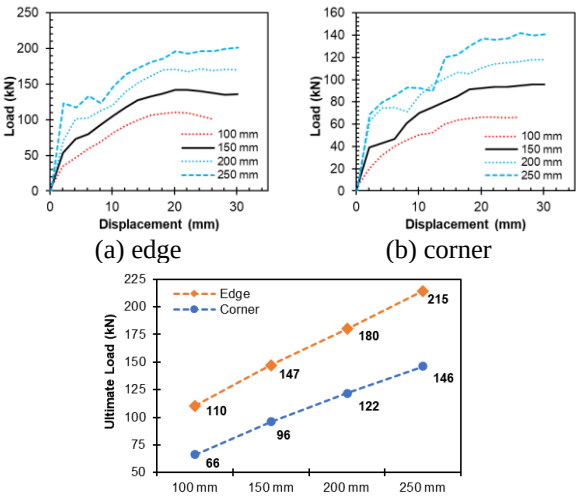

(a) edge (b) corner

(c) variation

Figure 14: Parametric investigations: effect of slab thickness

The failure load capacities of the slabs were found to increase steadily as the slab thickness was increased, in edge and corner loading cases, as shown in Figure 14 (a and b). When loaded at the edges, the ultimate load capacities were found to be 110 kN, 147 kN, 180 kN, and 215 kN, for thicknesses of 100 mm, 150 mm, 200 mm, and 250 mm, respectively Figure 14 (c). When loaded at the corners, the ultimate load capacities were found to be 66 kN, 96 kN, 122 kN, and 146 kN, for thicknesses of 100 mm, 150 mm, 200 mm, and 250 mm, respectively Figure 14 (c).

4.5 Effect of additional rebar grids

To study the effect of an additional rebar grid at the bottom half of the slab, four types of grids were developed, as shown in Figure 15.

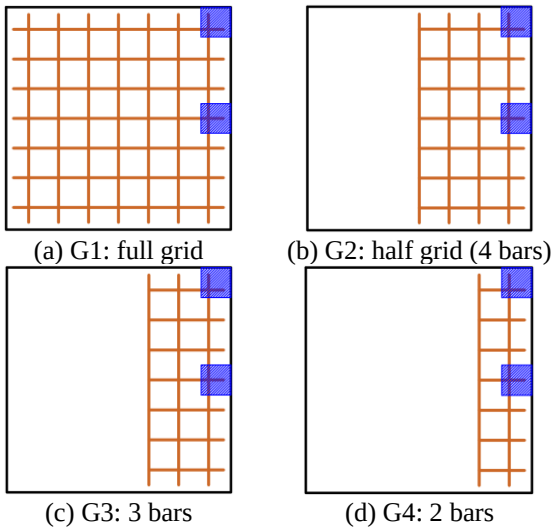

(a) G1: full grid (b) G2: half grid (4 bars)

(c) G3: 3 bars (d) G4: 2 bars

Figure 15: Configurations of the second rebar grid placed in the bottom half of the slab-on-ground

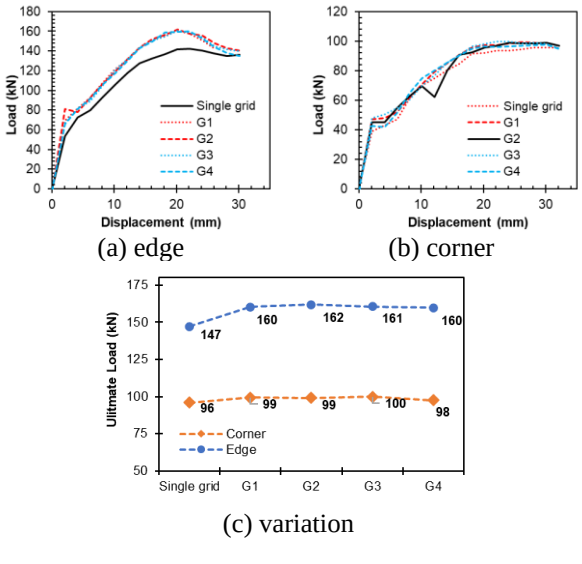

(a) edge (b) corner

(c) variation

Figure 16: Parametric investigations: effect of additional rebar grids

The provision of the addition was found to provide an advantage in the edge-loaded load. Irrespective of the type of grid used, an

increase of approximately 10% was observed, in the edge-loaded slab models (Figure 15 (a and c)).

However, no enhancement in performance was observed in the slab-on-ground slab loaded at the corner. It can thus be inferred that a bottom layer of reinforcement is only helpful when a punching shear mode of failure is involved. The mode of failure in the corner-loaded slab was predominantly flexural.

4.6 Effect of corner diagonal reinforcements

A simple yet effective way to improve the load-carrying capacity of GFRP bar-reinforced concrete slabs-on-ground (with 200 mm spacing) was investigated by placing 700 mm-long GFRP bars at the corners above the existing rebar grid, as shown in Figure 17.

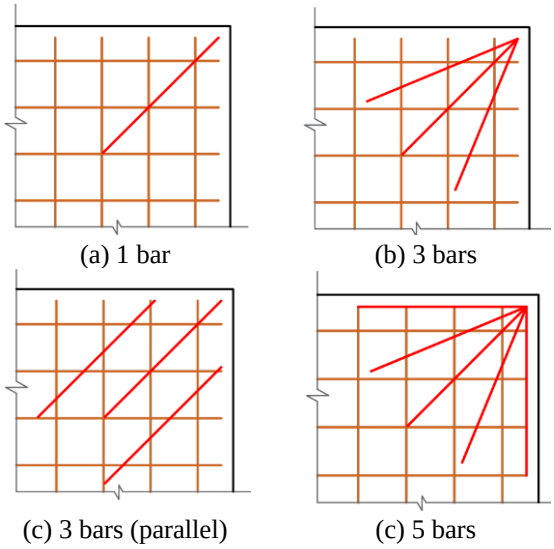

Figure 17: Configurations of corner reinforcing bars

Notable improvements in strength and stiffness were observed even when a single bar was placed. Placing one bar diagonally increased the capacity by 18%. Ultimate load capacities in control ("No diag."), "1 bar", "3 bars", "3 bars (parallel)" and "5 bars" configurations were observed to be 96 kN, 113 kN, 116 kN, 109 kN, and 115 kN, respectively, as shown in Figure 18.

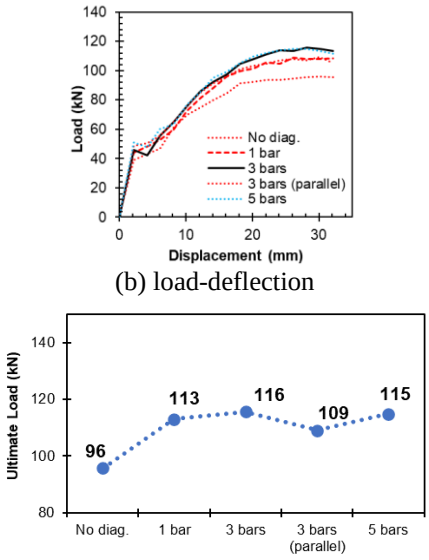

Figure 18: Parametric investigations: effect of corner diagonal reinforcements

5 COMPARISON OF RESULTS WITH DESIGN EQUATIONS

Punching shear capacity prediction equations for steel-reinforced concrete suspended slabs have been discussed extensively in several codes and guidelines, including ACI 440.11-22 [13], ACI 440.1R-15 [14], CSA S806-12 [15], and BS 8110 [16], besides models proposed by several researchers. Punching shear capacity on steel-reinforced concrete slabs-on-ground was proposed by The Concrete Society code TR 34 [17], as shown in Table 4. For GFRP bar-reinforced concrete slabs-on-ground, Al-Zahrani et al. [7] proposed an empirical equation for determining punching shear capacity, as shown in Table 4.

Numerical punching shear capacity results from three parameters of the present study: concrete compressive strength, rebar spacing, and slab thickness were used to compare the effectiveness of the empirical models. It is important to note that, the TR 34 [17] and Al-Zahrani et al. [7] models were developed for determining shear capacity at interior locations of slabs (away from edges and corners). However, the term $b_{o,2.0d}$ in both equations was appropriately calculated to accommodate reductions in capacity as much as possible.

Table 4: Punching shear capacity models for slabs-on-ground

Model	Equation
TR 34 [17]	$v_{R,dc} = \frac{0.18k_s}{\gamma_c}(100\rho_1 f_{ck})^{0.33} \geq 0.035k_s^{1.5} f_{ck}^{0.5}$ $k_s = 1+(200/d)^{0.5} \leq 2$; $\rho_1 = \sqrt{\rho_x \rho_y}$ ρ_x = reinforcement ratio in the *x*-direction ρ_y = reinforcement ratio in the *y*-direction f_{ck} = characteristic 28-day cylinder compressive strength (MPa)
Al-Zahrani et al. [7]	$V_c = \lambda_d \lambda_\rho \lambda_f \sqrt{f'_c} b_{o;2.0d} d$ $\lambda_d = 0.18\left[1+\left(\frac{200}{d}\right)^{0.25}\right]$ $\lambda_\rho = 1.15(100\rho)^{0.15}$; $\rho = A_r / A_g$ $\lambda_f = \left(\frac{E_f}{E_s}\right)^{0.2}$ (GFRP rebars) λ_f = 1.0 (steel rebars)

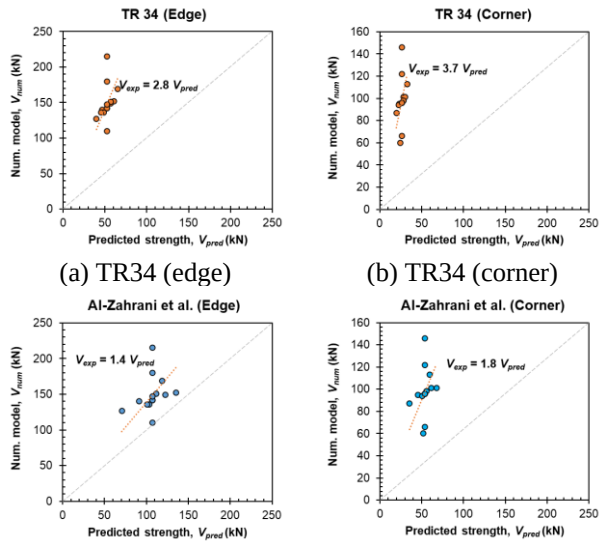

(a) TR34 (edge) (b) TR34 (corner)

(c) Al-Zahrani et al. [7] model (edge) (d) Al-Zahrani et al. [7] model (Corner)

Figure 19: Parametric investigations: effect of corner diagonal reinforcements

Figure 19 shows parity plots indicating the effectiveness of the empirical models, in which the "X-axis" is the predicted strength from the empirical models and the "Y-axis" is the strengths predicted by the validated numerical model. It is observed that the TR 34 [17] is more conservative than the Al-Zahrani et al. model [7], in both edge and corner loading scenarios. More numerical models and experimental results from literature can be used as a means to modify and enhance the model to be able to use reliably in problems involving edge and corner loading conditions.

6 CONCLUSIONS

1. Finite element models of GFRP bar-reinforced concrete slabs-on-ground subjected to concentrated loads at center, edge, and corner positions were developed in ABAQUS. The prediction of strength and load-displacement response in the slabs by the numerical model agreed well with the experimental results of 7 GFRP and steel-reinforced concrete slabs-on-ground, resting on a simulated soil subgrade. The validation model was used to study the effect of parameters such as concrete compressive strength, concrete tensile strength, rebar spacing, slab thickness, and the additional reinforcing bars for strengthening at edge and corner positions.
2. Concrete strength was found to play an important role in enhancing capacities at edge and corner positions. The effect of concrete compressive strength was more apparent at the edges, as compared to the corner position. Concrete tensile strength increased the ultimate strength and stiffness of the load-displacement curve, at both edge and corner positions.
3. Smaller spacings exhibited a notable increase in capacity at edge and corner positions. Although, no significant gain in strength was observed when the spacing was decreased from 300 mm to 250 mm, an increase of 24% was observed when the spacing was decreased to 100 mm.
4. Slab thickness played an important role in enhancing the ultimate load capacity of GFRP bar-reinforced concrete slabs-on-ground. Doubling the thickness from 100 mm to 200 mm resulted in 63% and 84% increases in ultimate load capacities at edge and corner positions, respectively.

5. The provision of additional rebar grids of various sizes played a significant role in enhancing the punching load capacity of the edge-loaded slabs. However, this addition did not strengthen corner positions. Interestingly, placing at least one diagonal bar at the corner on top of the existing rebar grid exhibited a significant increase in the capacity and stiffness of the slabs when loaded at the corner. This is simple and very effective means of increasing capacity at the corner positions.
6. Results from the study were used to compare the effectiveness of two punching shear capacity prediction models for slabs-on-ground from literature: TR 34 (steel) and Al-Zahrani et al. (GFRP). Parity plots revealed that models were conservative in their predictions. However, more numerical models and experimental results from literature can be used to modify and enhance these models to fit in edge and corner loading scenarios.

ACKNOWLEDGEMENTS

The authors gratefully acknowledge the financial support provided by Saudi Aramco under the Saudi Aramco contract No. 6600011900. The authors would like to thank the IRC for Construction and Building Materials, ARC for Metrology, Standards and Testing, and the Civil and Environmental Engineering Department at the King Fahd University of Petroleum and Minerals (KFUPM), Saudi Arabia for providing all the necessary support for conducting the research.

REFERENCES

[1] Nanni A., De Luca A., and Zadeh H.J., 2014. *Reinforced Concrete with FRP Bars Mechanics and Design. 1st ed.,* CRC Press.

[2] Benzecry V., Al-Khafaji A.F., Haluza R.T., Bakis C.E., Myers J.J., and Nanni A., 2021. Durability Assessment of 15- to 20-Year-Old GFRP Bars Extracted from Bridges in the US. I: Selected Bridges, Bar Extraction, and Concrete Assessment. *J. Compos. Constr.* **25**:04021007.

[3] Benmokrane B., Nazair C., Loranger M-A, and Manalo A., 2018. Field Durability Study of Vinyl-Ester–Based GFRP Rebars in Concrete Bridge Barriers. *J. Bridge Eng.* **23**:04018094.

[4] Behrouz Shafei, Brent Phares, Dikshant Saini, 2020. *Field Investigation of Bridge Deck Reinforced with Glass Fiber Reinforced Polymer (GFRP) Rebar. Minnesota, USA: Local Road Research Board*, Minnesota Department of Transportation.

[5] Kwak H-G, Seo Y-J, and Jung C-M, 2000. Effects of the slab casting sequences and the drying shrinkage of concrete slabs on the short-term and long-term behavior of composite steel box girder bridges. Part 1. *Eng. Struct.*, **22**:1453–66.

[6] Al-Humeidawi B.H., and Mandal P., 2014. Evaluation of performance and design of GFRP dowels in jointed plain concrete pavement – part 1: experimental investigation. *Int. J. Pavement Eng.* , **15**:449–59.

[7] Al-Zahrani M.M., Rahman M.K., Fasil M., Al-Abduljabbar S., Nanni A., Al-Osta M.A., et al., 2023. Punching shear capacity of GFRP bar-reinforced concrete slabs-on-ground. *Eng. Struct.* **289**:116285.

[8] Beverly P., and Walraven J.C., 2010. International Federation for Structural Concrete, International Federation for Structural Concrete, editors. *fib model code for concrete structures*. Ernst & Sohn.

[9] Wahalathantri B., Thambiratnam D., Chan T., and Fawzia S., 2011. A material model for flexural crack simulation in reinforced concrete elements using

ABAQUS. In: Cowled CJL, editor. *Proc. First Int. Conf. Eng. Des. Dev. Built Environ. Sustain. Wellbeing, Australia*, Queensland University of Technology, p. 260–4.

[10] Birtel V., and Mark P., 2006. Parameterised finite element modelling of RC beam shear failure, *ABAQUS users' conference*, Boston, USA, p. 95–108.

[11] Tabatabaei Aghda S.T., Ghanbari A., and Tavakoli Mehrjardi G., 2019. Evaluating the Applicability of Geocell-Reinforced Dredged Sand Using Plate and Wheel Load Testing. *Transp. Infrastruct. Geotechnol.* **6**:21–38.

[12] Smith I., 2021. *Smith's elements of soil mechanics. 10th edition.* Hoboken, NJ: Wiley-Blackwell.

[13] ACI Committee 440, 2022. *ACI CODE 440.11-22: Building Code Requirements for Structural Concrete Reinforced with Glass Fiber-Reinforced Polymer (GFRP) Bars-Code and Commentary. 1st printing*. Farmington Hills, MI: American Concrete Institute (ACI).

[14] ACI, 2015. *ACI 440.1R-15: Guide for the design and construction of structural concrete reinforced with fiber-reinforced polymer (FRP) bars. 1st printing.* Farmington Hills, MI: American Concrete Institute.

[15] CSA, 2012. *CSA S806-12: Design and construction of building components with fiber reinforced polymers.* Canadian Standards Association (CSA).

[16] British Standards Institution (BSI). BS 8110-1:1997, 1997. *Structural use of concrete — Part 1: Code of practice for design and construction.* London.

[17] Concrete Society Project Steering Committee, Design sub-group. *Technical Report 34: Concrete Industrial Ground Floors - A guide to design and construction. 4th ed.* The Concrete Society.